Line Shapes in the Radio-Frequency Size Effect of Metals*

G. E. Juras†
The James Franck Institute and Department of Physics, The University of Chicago, Chiczgo, Illinois 60637
(Received 9 May 1969)

The nonmonotonic behavior of the surface impedance of a thin metal plate excited by a high-frequency electromagnetic field has been examined as a function of a dc magnetic field imposed parallel to the faces of the plate. The line shapes of this rf size effect have been calculated for different types of electronic orbits and for different modes of excitation of the plate by the high-frequency field. The spatial distribution of the electric field, including the field "splashes" associated with the anomalous penetration of the electric field into the sample due to chains of trajectories, was obtained self-consistently from the integrodifferential equation which results after combining Maxwell's equations with Chambers's solution to the Boltzmann equation under the nonlocal conditions of the anomalous skin effect, assuming diffuse scattering at the surfaces and a constant relaxation time for bulk scattering. Qualitative comparison with experiment has been made.

I. INTRODUCTION

ELECTROMAGNETIC fields incident on the surface of a metal with frequencies less than the plasma frequency of the free charge carriers of the metal (conduction electrons) do not penetrate deep into the bulk of the metal; the small amount of field energy that does enter into the sample is confined to a very thin layer of surface current within the skin depth δ ($\delta \approx 10^{-3}$–10^{-4} cm for pure metals at low temperatures and radio frequencies). The changes that the amplitude and phase of the incident wave suffer upon reflection, albeit small, can be measured experimentally. These changes are specified by the surface impedance Z of the metal[1,2] defined as the ratio of the tangential electric and magnetic fields just inside the surface of the metal. The real part of Z, the surface resistance, measures the fraction of incident power that is lost to the sample either through Joule heating or through collisionless mechanisms of direct interaction between the charge carriers and the different Fourier components of the field.[3] The imaginary part of Z, the surface reactance, is related to the phase shift of the reflected wave or equivalently the frequency change of the exciting resonant circuit, i.e., the inductance change of the exciting coil.[4]

In very pure metals and at liquid-helium temperatures, the electrons which contribute to the conductivity of the metal are localized on the Fermi surface, the scattering with the lattice is reduced, and the mean free path l may be as large as several millimeters, i.e., many times larger than the skin depth δ. The current density and the electric field are no longer related by the usual local form of Ohm's law

$$\mathbf{j}(\mathbf{r}) = \boldsymbol{\sigma} \cdot \mathbf{E}(\mathbf{r}); \tag{1.1}$$

instead, the current density at a point $\mathbf{r}$ in the metal is defined by the electric field in a region with dimensions of the order of l. The conductivity $\boldsymbol{\sigma}$ is no longer a constant of the metal; rather, it depends on the spatial distribution of the electric field.[5,6] In these anomalous skin-effect conditions and in the presence of an external magnetic field, sharply defined changes, hereafter referred to as *resonances* or *singularities*, occur in the surface impedance as a function of either frequency or magnetic field.

The Azbel'-Kaner resonance[7] is an example of a temporal resonance in which both the surface resistance and the surface reactance show minima at those values of the external frequency which are equal to (or a multiple of) the cyclotron frequency of extremal electronic orbits on the Fermi surface.

The rf size effect (RFSE), first discovered by Gantmakher in tin,[8] is a spatial resonance which occurs in the surface impedance Z of a thin metal plate (thickness approximately equal to 1 mm) excited by a high-frequency electromagnetic field (frequency approximately equal to 1 MHz) when Z is measured as a function of magnetic field applied either parallel or at an angle with respect to the faces of the sample.

Some of the RFSE singularities are geometric in character and occur primarily at those critical values of the magnetic field which make the dimensions of a large group of electron trajectories nearly equal to the thickness of the sample. Measurement of those critical

* Research supported in part by the U. S. Office of Naval Research and the National Aeronautics and Space Administration.
† Submitted in partial fulfillment of the requirements for the Ph.D. degree at the University of Chicago.
[1] L. D. Landau and I. M. Lifshitz, *Electrodynamics of Continuous Media* (Addison-Wesley Publishing Co., Reading, Mass., 1960), p. 280.
[2] C. Kittel, *Quantum Theory of Solids* (Wiley-Interscience, Inc., New York, 1963), p. 308.
[3] E. A. Kaner and V. G. Skobov, Advan. Phys. **17**, 605 (1968); Usp. Fiz. Nauk **89**, 367 (1966) [English transl.: Soviet Phys.—Usp. **9**, 480 (1967)].
[4] J. F. Cochran and C. A. Shiffman, Phys. Rev. **140**, A1678 (1965).
[5] A. B. Pippard, Proc. Roy. Soc. (London) **A191**, 385 (1947).
[6] G. E. H. Reuter and E. H. Sondheimer, Proc. Roy. Soc. (London) **A195**, 336 (1948).
[7] M. Ya. Azbel' and E. A. Kaner, Zh. Eksperim. i Teor. Fiz. **32**, 896 (1957) [English transl.: Soviet Phys.—JETP **5**, 730 (1957)]; Phys. Chem. Solids **6**, 113 (1957).
[8] V. F. Gantmakher, Zh. Eksperim. i Teor. Fiz. **42**, 1416 (1962); **43**, 345 (1962); **44**, 811 (1963) [English transls.: Soviet Phys.—JETP **15**, 982 (1962); **16**, 247 (1962); **17**, 549 (1963)].

magnetic field values, at which the relatively easy to analyze resonances appear, yields extremal calipers of the Fermi surface of the metal, thus elucidating our understanding of its band structure (see Ref. 9, for example).

Other RFSE resonances are due to anomalous penetration of the electric field into the sample.[10–12] This anomalous penetration of the electric field into the metal in anomalous skin-effect conditions is connected with the fact that individual effective electrons, i.e., electrons which move parallel to the metal surface when they are in the skin layer, can carry current away from the skin layer and reproduce it deep within the interior of the metal, thus forming narrow "splashes" or sheets of electric field and current which damp slowly into the metal. This type of anomalous penetration is to be distinguished from the anomalous penetration of the electromagnetic field into a metal due to resonant excitation of the collective motion of the electron-hole plasma by an external wave.[3]

As has been discussed in earlier works (see Ref. 13, for example) there are essentially two different mechanisms of selection of effective electrons by the external magnetic field in order for them to form field splashes within the interior of the metal.

In the first mechanism, the magnetic field is applied parallel to the faces of the sample. The electrons on the extremal sections of a closed Fermi surface which move nearly parallel to the surface when they are in the skin layer describe a finite trajectory in real space and create a current sheet at a depth d_0 approximately equal to the diameter of the trajectory, namely, at the depth where the velocity of the extremal electrons is again parallel to the surface. This current splash, which is a narrow image of the surface current layer, serves as the exciting skin layer of those bulk electrons which pass through it with their velocities parallel to the surface. These electrons in turn create another current splash at $2\times d_0$, which excites other electrons deeper in the metal, and so forth, thus creating a chain of effective trajectories. This "trajectory chain" mechanism for anomalous penetration of the field in the metal was discovered experimentally in Sn by Gantmakher.[8]

The second mechanism of electron selection and splash formation is connected with the focusing of effective electrons during their drifting motion into a metal in a magnetic field inclined with respect to the surface. The splashes appear at depths which are integral multiples of u, where u is an extreme value of the normal-to-the-surface projection of the mean electron displacement in one cyclotron period. The extremal values of u correspond to conduction electrons at the limiting points of the Fermi surface, which are defined as the points of contact of the Fermi surface with tangent planes perpendicular to the magnetic field. Near these limiting points the electron velocity is almost parallel to the magnetic field and the electron trajectory is a helix with a very long pitch. Splashes are expected to occur again at those regions of the metal where a large number of electrons have their velocities parallel to the surface. RFSE singularities due to limiting point electron trajectories were first discussed by Gantmakher and Kaner.[14]

For the existence of the anomalous penetration effects due to either of the above mechanisms, the following conditions must be satisfied:

$$\delta \ll D \tag{1.2a}$$

and

$$D \ll l, \tag{1.2b}$$

where D is the characteristic dimension of an extremal electron trajectory in the magnetic field. Condition (1.2a) ensures anomalous skin-effect conditions for the entire characteristic dimension of the electron trajectory, while condition (1.2b) ensures that the electrons will make many cyclotron trajectories before scattering.

In order to explain in detail the line shapes of the many singularities of the RFSE, the inhomogeneity of the electric field in the metal should be combined self-consistently with the dispersion law of the electrons and the nature of electronic scattering at the surfaces.

The dispersion law defines the type of trajectories that the electrons describe in the magnetic field. The topology of the electronic trajectories in turn affects very strongly the magnetic field dependence of the response of the system to an external electric field.

The scattering with the surfaces affects the "effectiveness" of the electrons to respond to the high-frequency field. Those electrons which spend a large fraction of their mean free paths inside the skin layer and do not collide with the surfaces of the sample will be more effective in conducting current than the electrons which collide with either or both surfaces during one cyclotron period. The relative number of effective-versus-ineffective electrons due to surface scattering is a strong function of magnetic field. This follows from the fact that the size of the electronic trajectories is inversely proportional to the magnetic field. The diameter of a circular free-electron trajectory is $2(ch/e)k_F/H$, where k_F is the Fermi wave vector, and it is equal to the thickness of the sample d at the critical value of the magnetic field H_0, where

$$H_0 = 2(ch/e)(k_F/d).$$

[9] R. C. Jones, R. G. Goodrich, and L. M. Falicov, Phys. Rev. **174**, 672 (1968).

[10] M. Ya. Azbel', Zh. Eksperim. i Teor. Fiz. **39**, 400 (1960) [English transl.: Soviet Phys.—JETP **12**, 283 (1961)].

[11] E. A. Kaner, Zh. Eksperim. i Teor. Fiz. **44**, 1036 (1963) [English transl.: Soviet Phys.—JETP **17**, 700 (1963)].

[12] E. A. Kaner and V. L. Fal'ko, Zh. Eksperim. i Teor. Fiz. **49**, 1895 (1965) [English transl.: Soviet Phys.—JETP **22**, 1294 (1966)].

[13] E. A. Kaner, Physics **3**, 285 (1967).

[14] V. F. Gantmakher and E. A. Kaner, Zh. Eksperim. i Teor. Fiz. **45**, 1430 (1963) [English transl.: Soviet Phys.—JETP **18**, 988 (1964)].

For magnetic field values smaller than H_0, an effective electron becomes ineffective during one cyclotron period since it scatters with the opposite surface of the plate. For magnetic field values greater than H_0, an effective electron remains effective during its entire mean free time τ ($\tau \gg 1/\Omega$, where Ω is the cyclotron frequency) in that it is able to return to the skin layer many times and thus to interact effectively with the large-amplitude field there.

The inhomogeneity of the electric field in the sample affects the line shape of the RFSE resonances in the following important way: An effective electron which moves parallel to the skin layer and thus spends a good fraction of its mean free time in the skin layer may again move parallel to the surface at other portions of its trajectory in the bulk of the sample or, as in the case of bilateral excitation (see Fig. 1), in the skin layer of the other surface. The coupling of the electric field with the electronic motion in these effective regions of the trajectory is strongest if the velocity of the electron is in phase [meaning that the dot product $\mathbf{v}\cdot\mathbf{E}$ integrated over the effective region is maximum—see (2.16a)] with the electric field and the field amplitude there is relatively large as compared with the amplitude at other regions of the sample. Since the magnetic field determines the size of the trajectories and thus affects the way in which the effective regions of the trajectories sample the electric field, the coupling between the electrons and the electric field is a strong function of the applied magnetic field. It should be recalled at this point that it is the same electron trajectories, modified as they are by the magnetic field, which in a self-consistent manner induce the large amplitude regions of the field in the interior of the sample by the penetration mechanisms already discussed.

To observe the RFSE singularities experimentally, various modes of excitation of the thin metal plate by the rf electromagnetic wave may be employed; three such modes are shown schematically in Fig. 1. In the bilateral antisymmetric mode of excitation, the metal plate is placed inside an inductance coil which is made part of the tank circuit of an oscillator. If a change in magnetic field affects the surface impedance of the sample, then this leads to a detectable change in the characteristics of the resonator. The driving currents are in opposite directions in the two skin layers of the sample. In the bilateral symmetric excitation the driving currents are in the same direction in both skin layers of the sample. In the case of unilateral excitation the metal plate is excited by a flat spiral coil placed on one surface of the specimen. The impedance is either monitored on the driving side of the slab[15] or a transmission measurement is made[16] in which the transmitted radiation is detected by a radio receiver placed at the other side of the slab.

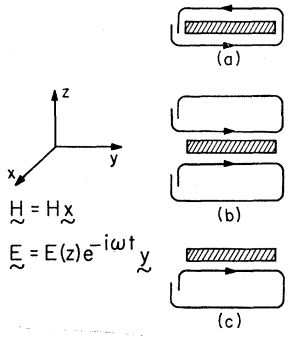

FIG. 1. Schematic of three possible modes of excitation of a thin metal plate by a rf electromagnetic field, in the presence of an external magnetic field **H** applied parallel to the faces of the plate: (a) bilateral, antisymmetric excitation, (b) bilateral, symmetric excitation, and (c) unilateral excitation.

In all modes of excitation the derivative of the surface impedance with respect to magnetic field is measured experimentally by modulating the magnetic field at an audio frequency and detecting the resulting signal coherently.[17] Variations of the detected voltage amplitude are proportional to the magnetic field derivative of the real part of Z. Changes in the oscillator frequency are proportional to the field derivative of the imaginary part of Z. In a typical RFSE experiment, the metal plate has a thickness $d \approx 10^{-2}$–10^{-1} cm, while the frequency of the exciting electromagnetic wave $\omega/2\pi$ is of the order of a few MHz, i.e., it is high enough so that $\delta \ll d$, and yet low enough so that it is much smaller than the cyclotron frequency of the carriers:

$$\Omega/2\pi = eH/2\pi mc \approx 2.80H \text{ MHz}, \quad H \text{ in Oe}.$$

The condition $\omega \ll \Omega$ ensures that the carriers experience a nearly static field in the skin layers every time they pass through them. A mean free path about as large as the thickness of the plate is sufficient for the observation of the RFSE singularities.

In the review articles by Gantmakher,[18] Kaner and Gantmakher,[19] and Walsh,[20] the various aspects of the RFSE are discussed in detail with extensive reference lists to most of the experimental and theoretical contributions in this field.

Kaner and Fal'ko[21] have calculated the line shapes of the surface impedance anomalies in the unilateral-excitation case for circular electron trajectories and some approximate, not self-consistent, distributions of the electric field in the metal. Koch and Wagner[15] performed the corresponding experiment in potassium, and they report rough agreement between the theoretical and experimental line shapes; however, the

[15] T. K. Wagner and J. F. Koch, Phys. Rev. **165**, 885 (1967).
[16] C. C. Grimes, in *Proceedings of the Ninth International Conference on Low-Temperature Physics, Columbus, Ohio*, edited by J. G. Daunt *et al.* (Plenum Press, Inc., New York, 1965), p. 723.
[17] M. S. Khaikin, Pribory i Tekhn. Eksperim. **3**, 95 (1961).
[18] V. F. Gantmakher, in *Progress in Low-Temperature Physics*, edited by C. J. Gorter (North-Holland Publishing Co., Amsterdam, 1966), Vol. 5, p. 181.
[19] E. A. Kaner and V. F. Gantmakher, Usp. Fiz. Nauk **94**, 193 (1968) [English transl.: Soviet Phys.—Usp. **11**, 81 (1968)].
[20] W. M. Walsh, Jr., in *Solid State Physics*, edited by J. F. Cochran and R. R. Haering (Gordon and Breach, Science Publishers, Inc., New York, 1968), Vol. 1, p. 127.
[21] E. A. Kaner and V. L. Fal'ko, Zh. Eksperim. i Teor. Fiz. **51**, 586 (1966) [English transl.: Soviet Phys.—JETP **24**, 392 (1967)].

observed discrepancies are large enough to indicate that the approximations (such as neglect of radiation from the second surface) made in the theory of Kaner and Fal'ko, which is not the complete solution to the full boundary-value problem, may well be significant. The line shapes for the oblique field geometry have been calculated by Kaner.[13]

In this work an attempt is made to solve self-consistently the complete boundary-value problem of the RFSE for an arbitrary Fermi surface and different modes of excitation of the sample by the external rf field, assuming diffuse scattering at the surfaces and a uniform relaxation time for bulk scattering. Only the case of magnetic fields parallel to the surface is considered, with electric fields transversely polarized with respect to **H**.

In Sec. II Maxwell's equations are combined with Chambers's solution[22] of the Boltzmann equation to produce an integrodifferential equation which is to be solved for the unknown distribution of the electric field in the sample, subject to appropriate boundary conditions. In Sec. III a numerical procedure is developed by which the integrodifferential equation of Sec. II may be solved approximately. Some model calculations are carried out and the resulting curves are discussed in Sec. IV.

II. THEORY

To determine the electric field distribution inside the metal it is necessary to solve Maxwell's equations together with the kinetic equation for the electron distribution function of the metal, subject to appropriate boundary conditions; of course, the dynamics of electrons in an external magnetic field have to be taken into account explicitly.

For a semiclassical electron with charge $-|e|$, position $\mathbf{r}$, quasimomentum $\mathbf{p}$, and energy $\mathcal{E}(\mathbf{p})$, the equation of motion in a fixed magnetic field $\mathbf{H}$ is

$$\dot{\mathbf{p}}=-(|e|/c)\mathbf{v}\mathbf{H}, \tag{2.1a}$$

with the electron velocity given by

$$\mathbf{v}=\dot{\mathbf{r}}=\partial\mathcal{E}/\partial\mathbf{p}. \tag{2.1b}$$

The integrals of motion are

$$\mathcal{E}(\mathbf{p})=\mathcal{E}=\text{const}, \tag{2.2a}$$

$$p_H=\mathbf{p}\cdot\mathbf{H}/H=\text{const}, \tag{2.2b}$$

and they define the electronic orbits in momentum space as simply intersections of the energy surface $\mathcal{E}(\mathbf{p})=\mathcal{E}$ by planes normal to $\mathbf{H}$, insofar as the magnetic field only drives the electrons around their orbits without change in energy, leaving the projection of their momentum along $\mathbf{H}$ conserved. The electromagnetic field is assumed not to disturb the topology of the orbits.

[22] R. G. Chambers, Proc. Roy. Soc. (London) **A65**, 458 (1952); **A238**, 344 (1966).

As is evident from (2.1a) and (2.1b) upon integration, the momentum-space *orbits* and the projections of the real-space *trajectories* on the plane perpendicular to $\mathbf{H}$ are similar, the similarity factor being eH/c, and are rotated by $\frac{1}{2}\pi$ about the direction of $\mathbf{H}$ relative to each other. Some real-space trajectories and the ways in which they span a thin plate are shown in Fig. 2.

The size of a trajectory in a given direction is inversely proportional to the magnetic field. From (2.1a), (2.1b), and $\mathbf{H}=H\mathbf{x}$, as in the geometry of Fig. 1, the dimension of a closed trajectory in the z direction is

$$z_{\max}-z_{\min}=|(c/eH)(p_{y,\max}-p_{y,\min})|, \tag{2.3}$$

with a similar expression for the dimension in the y direction.

The cyclotron frequency of an electron describing a closed orbit is given by

$$\Omega(\mathcal{E},p_x)=|e|H/m^*(\mathcal{E},p_x)c, \tag{2.4a}$$

where the cyclotron mass is defined to be

$$m^*(\mathcal{E},p_x)=(1/2\pi)\partial S(\mathcal{E},p_x)/\partial\mathcal{E}; \tag{2.4b}$$

here $S(\mathcal{E},p_x)$ is the cross-sectional area of the energy surface $\mathcal{E}(p)=\mathcal{E}$ intersected by a plane normal to $\mathbf{H}$ at a given p_x.

If the displacement current $\dot{D}$ in a metal is neglected (conductivities of good conductors are much larger than radio frequencies: $\sigma\approx10^{18}$ sec^{-1}, $\omega\approx10^{6}$ sec^{-1}), then Maxwell's curl equations have the form

$$\begin{aligned}\nabla\times\mathbf{H}&=(4\pi/c)\mathbf{j},\\ \nabla\times\mathbf{E}&=-(1/c)\dot{\mathbf{H}}.\end{aligned} \tag{2.5}$$

Assuming a time variation of the form $e^{-i\omega t}$ for the fields and eliminating $\mathbf{H}$ from (2.5), we obtain

$$\partial^2E_\alpha(z)/\partial z^2=-i(4\pi\omega/c^2)j_\alpha(z),\quad \alpha=x,y \tag{2.6}$$

where the system of coordinates is shown in Fig. 1. We have neglected the variation of the fields in x and y since the wavelength of rf radiation is much larger

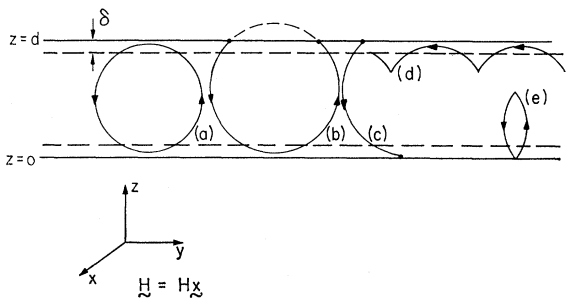

FIG. 2. Electron trajectories spanning a thin metal plate in the presence of an external magnetic field: (a) an effective electron which describes a bulk trajectory, (b) an effective electron in the skin layer at the surface $z=0$ which becomes ineffective during one cyclotron period because of diffuse scattering at $z=d$, (c) an ineffective electron which collides with both surfaces, (d) an effective open trajectory, and (e) an ineffective "lens" trajectory.

than δ, the distance of spatial variation of the fields is the z direction.

From the continuity equation we have

$$j_z(z)=0. \tag{2.7}$$

Owing to the fact that the main contribution to the current density is made by electrons moving almost parallel to the surface of the metal, we can assume that $E_z=0$ and thus disregard (2.7) in later considerations.[7]

The current density in (2.6) is defined as

$$j_\alpha(z)=-2\frac{|e|}{(2\pi\hbar)^3}\int_{\text{all p}} d^3p\, v_\alpha(\mathbf{p})f(z;\mathbf{p}), \tag{2.8}$$

where $f(z;\mathbf{p})$ is the perturbation addition to the equilibrium Fermi distribution function,

$$f_0(\mathcal{E})=[\exp(\mathcal{E}-\mathcal{E}_F/kT)+1]^{-1}, \tag{2.9}$$

due to the influence of the external fields. The velocity of the electrons $\mathbf{v}(\mathbf{p})$ is defined by (2.1b) as the gradient of the $\mathcal{E}(\mathbf{p})=\mathcal{E}$ surface, where $\mathcal{E}(\mathbf{p})$ is the dispersion law of the electrons, i.e., the relation between the quasiparticle energy $\mathcal{E}$ and their quasimomentum $\mathbf{p}\cdot\mathcal{E}_F(T)$ is the chemical potential of the electrons, k is the Boltzmann constant, T is absolute temperature, and the factor of 2 in (2.8) is due to the electron-spin degeneracy.

The kinetic equation for $f(z;\mathbf{p})$, linearized in the electric field $\mathbf{E}$, is[7]

$$\partial f/\partial\varphi+(v_z/\Omega)\partial f/\partial z+\gamma f=(|e|/\Omega)\mathbf{v}\cdot\mathbf{E}\partial f_0/\partial\mathcal{E}, \tag{2.10}$$

where the independent variables are the coordinate z along the inward normal of the metal surface $z=0$, the energy of the electrons $\mathcal{E}$, the conserved component of the quasimomentum p_x, and the dimensionless "orbit" or "phase" variable $\varphi=\Omega t$ in place of the real time t. In terms of these variables, the element of volume in momentum space is given by $dp_xdp_ydp_z=|m^*|dp_xd\mathcal{E}d\varphi$, whose Jacobian is the cyclotron mass $|m^*|$.

The quantity γ in (2.10), defined by

$$\gamma(\mathbf{p})f=\frac{1}{\Omega}[(\partial f/\partial t)_{\text{coll}}-i\omega f], \tag{2.11a}$$

reduces to

$$\gamma(\mathbf{p})=[\Omega\tau(\mathbf{p})]^{-1}-i\omega/\Omega \tag{2.11b}$$

in the relaxation-time approximation. Justification for the introduction of a relaxation time into the anomalous skin-effect problem has been given in Ref. 7. Since in all of the subsequent model calculations we assume that the relaxation time for bulk scattering is constant over the entire Fermi surface and equal to τ, the quantity γ reduces to

$$\gamma\rightarrow 1/\Omega\tau \tag{2.11c}$$

in the case of low frequencies ($\omega\ll\Omega$, $\omega\ll 1/\tau$).

The electrons are assumed to scatter diffusely at the surfaces of the plate (this was thought to be almost always the case[23,24]; see, however, Ref. 25):

$$\begin{aligned} f(0;\mathbf{p})|_{vz>0}&=0,\\ f(d;\mathbf{p})|_{vz<0}&=0. \end{aligned} \tag{2.12}$$

After colliding with the surfaces the electrons are scattered into the equilibrium distribution $f_0(\mathcal{E})$, i.e., the perturbation addition to the distribution function due to the external fields becomes zero.

The solution of the Boltzmann equation (2.10), subject to the boundary conditions (2.12) for a thin plate, is the following (see Ref. 26, for example):

$$f(z;\mathbf{p})=\frac{|e|}{\Omega}\frac{\partial f_0}{\partial\mathcal{E}}\int_{\lambda(z;\mathbf{p})}^{\varphi} d\varphi'\exp[-\gamma(\varphi-\varphi')]\mathbf{v}(\varphi',p_x,\mathcal{E})\cdot\mathbf{E}\left(z-\frac{1}{\Omega}\int_{\varphi'}^{\varphi} d\varphi''v_z(\varphi'',p_x,\mathcal{E})\right), \tag{2.13}$$

where $\lambda(z;\mathbf{p})$ is the "time" immediately preceding φ that an electron collided with either boundary, if at "time" φ it is at a depth z of the plate with momentum $\mathbf{p}$.[27] Formally, $\lambda(z;\mathbf{p})$ satisfies the equation

$$z-\frac{1}{\Omega}\int_{\lambda(z;\mathbf{p})}^{\varphi} d\varphi''\,v_z(\varphi'',p_x,\mathcal{E})=0,\quad \lambda(z;\mathbf{p})\leq\varphi, \tag{2.14a}$$

if the electron started at the boundary $z=0$, or the equation

$$z-\frac{1}{\Omega}\int_{\lambda(z;\mathbf{p})}^{\varphi} d\varphi''\,v_z(\varphi'',p_x,\mathcal{E})=d,\quad \lambda(z;\mathbf{p})\leq\varphi, \tag{2.14b}$$

if the electron collided with the surface $z=d$ before reaching z at "time" φ. Obviously, we have

$$\begin{aligned} &\lambda(0;\varphi,p_x,\mathcal{E})=\varphi,\quad v_z>0\\ \text{and}\qquad &\\ &\lambda(d;\varphi,p_x,\mathcal{E})=\varphi,\quad v_z<0. \end{aligned} \tag{2.14c}$$

The meaning of $\lambda(z;\mathbf{p})$ is made more explicit in Fig. 3. If neither (2.14a) nor (2.14b) is satisfied, then

$$\lambda(z;\mathbf{p})=-\infty, \tag{2.14d}$$

and the electron at a depth z with momentum $\mathbf{p}$ never collides with either surface; in this case (2.13) reduces to Chambers's solution of the Boltzmann equation[22] for an infinite medium.

In the case of periodic bulk trajectories which never collide with either surface, the integral of (2.13) reduces

[23] R. G. Chambers, Proc. Roy. Soc. (London) **A215**, 481 (1952).
[24] K. Fuchs, Proc. Cambridge Phil. Soc. **34**, 100 (1938).
[25] J. F. Koch, in *Solid State Physics*, edited by J. F. Cochran and R. R. Haering (Gordon and Breach, Science Publishers, Inc., New York, 1968), Vol. 1, p. 253.
[26] E. A. Kaner, Zh. Eksperim. i Teor. Fiz. **34**, 658 (1958) [English transl.: Soviet Phys.—JETP **7**, 454 (1958)].
[27] P. Bloomfield, Physica **32**, 1189 (1966).

to an integral over one period only:

$$\int_{-\infty}^{\varphi} d\varphi' \cdots = [1-\exp(-\gamma\varphi_0)]^{-1} \int_{\varphi-\varphi_0}^{\varphi} d\varphi' \cdots , \quad (2.15)$$

where φ_0 is the period of the orbit.

Equation (2.13) has the following simple content: An electron with energy $\mathcal{E}$ and momentum p_x along the magnetic field passes through the plane z of the conductor at the "time" φ after having been scattered into a single trajectory at an earlier "time" φ' and at the depth

$$z' = z - \frac{1}{\Omega} \int_{\varphi'}^{\varphi} d\varphi''\, v_z(\varphi'', p_x, \mathcal{E})$$

of the conductor thus receiving from the electric field at z' during the time $d\varphi'/\Omega$ an energy increment

$$\Delta\mathcal{E} = |e|\mathbf{v}(\varphi', p_x, \mathcal{E}) \cdot \mathbf{E}\left(z - \frac{1}{\Omega}\int_{\varphi'}^{\varphi} d\varphi''\, v_z(\varphi'', p_x, \mathcal{E})\right)\frac{d\varphi'}{\Omega} \quad (2.16a)$$

with a probability of reaching (z,φ) without scattering equal to

$$\exp[-\gamma(\varphi-\varphi')]. \quad (2.16b)$$

The perturbed distribution function is then the integral over all the electrons which scattered into the trajectory at (z',φ') with energy $\mathcal{E}-\Delta\mathcal{E}$, weighted by their probability of reaching (z,φ).

From (2.8) and (2.13) the current density at z becomes

$$j_\alpha(z) = 2\frac{e^2}{(2\pi\hbar)^3} \int d\mathcal{E}\left(-\frac{\partial f_0}{\partial \mathcal{E}}\right) \int dp_x \frac{m^*}{\Omega} \int d\varphi\, v_\alpha(\varphi, p_x, \mathcal{E}) \times \int_{\lambda(z;\varphi,p_x,\mathcal{E})}^{\varphi} d\varphi' \exp[-\gamma(\varphi-\varphi')]\mathbf{v}(\varphi', p_x, \mathcal{E}) \cdot \mathbf{E}\left(z - \frac{1}{\Omega}\int_{\varphi'}^{\varphi} d\varphi''\, v_z(\varphi'', p_x, \mathcal{E})\right). \quad (2.17)$$

This is the nonlocal form of Ohm's law, which is to be used instead of (1.1) and which relates the current density at z through an integral conductivity operator with the electric field at another point of the metal plate within the region $(z_{\min}, z_{\max})$, where

$$z_{\min} = \max\{0, z-z_0\}, \qquad z_{\max} = \min\{d, z+z_0\}, \quad (2.18)$$

and z_0 is the dimension (in the z direction) of the maximum trajectory in the total electron distribution.

From the steplike character of the equilibrium distribution function at low temperatures we have that

$$(-\partial f_0/\partial\mathcal{E}) = \delta(\mathcal{E}-\mathcal{E}_F), \quad (2.19)$$

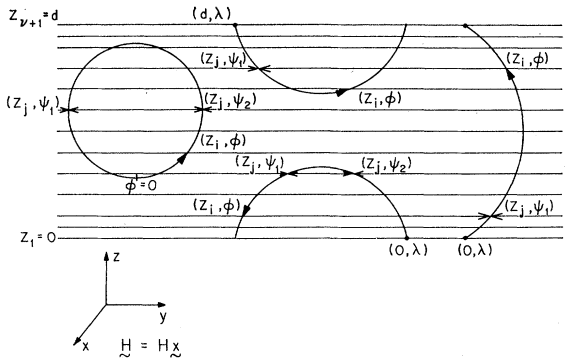

FIG. 3. Coordinate mesh used in the reduction of the integrodifferential equation (2.25) into the system (3.4) of $\nu-1$ linear, algebraic equations. Before reaching the depth z_i at "time" φ the electron crossed the plane z_j at "time (s)" ψ_s. The instant of the last collision with the surface at $z=0$ (or $z=d$) is λ. The origin $\varphi=0$ is chosen to correspond to the point on the trajectory with the lowest z value.

and the integration over energy in (2.17) can be eliminated; we need only integrate over the Fermi surface, i.e., integrate over all trajectories that pass through z with energy $\mathcal{E}_F$, momentum p_x along the magnetic field, and velocity direction characterized by φ.

By substituting the current density (2.17) in Maxwell's equations (2.6) the following integrodifferential equation results:

$$\frac{\partial^2 E_\alpha(z)}{\partial z^2} = -i\int_0^d K_{\alpha\beta}(z,\xi)E_\beta(\xi), \quad (2.20)$$

in which the kernel $K_{\alpha\beta}(z,\xi)$, which depends implicitly on the magnetic field $\mathbf{H}$, is the integral

$$K_{\alpha\beta}(z,\xi) = \frac{8\pi\omega e^2}{c^2(2\pi\hbar)^3} \int dp_x \frac{m^*}{\Omega} \int d\varphi\, \Lambda_{\alpha\beta}(z,\xi;\varphi,p_x), \quad (2.21a)$$

with the restriction that

$$K_{\alpha\beta}(z,\xi) = 0 \quad \text{for} \quad \xi \langle z_{\min}, \xi \rangle z_{\max}, \quad (2.21b)$$

i.e., the range of the kernel is of the order of the characteristic dimensions of the trajectories in the z direction, provided $l \gg |z_{\max}-z_{\min}|$.

The function $\Lambda_{\alpha\beta}(z,\xi;\varphi,p_x)$, defined by

$$\Lambda_{\alpha\beta}(z,\xi;\varphi,p_x) = v_\alpha(\varphi,p_x) \int_{\lambda(z;\varphi,p_x)}^{\varphi} d\varphi' \exp[-\gamma(\varphi-\varphi')]v_\beta(\varphi',p_x) \times \delta\left[\xi - z + \frac{1}{\Omega}\int_{\varphi'}^{\varphi} d\varphi'' v_z(\varphi'',p_x)\right], \quad (2.22a)$$

reduces to

$$\Lambda_{\alpha\beta}(z,\xi;\varphi,p_x) = v_\alpha(\varphi,p_x)\sum_s \frac{\exp[-\gamma(\varphi-\psi_s)]v_\beta(\psi_s,p_x)}{|(1/\Omega)v_z(\psi_s,p_x)|}, \quad (2.22b)$$

using the properties of the δ function; here the summation over s is over all the zeros $\psi_s(z,\xi;\varphi,p_x)$ of the argument of the δ function which exist between φ and $\lambda(z;\varphi,p_x)$:

$$\xi-z+\frac{1}{\Omega}\int_{\psi_s(z,\xi;\varphi,p_x)}^{\varphi} d\varphi'' v_z(\varphi'',p_x)=0, \quad (2.23)$$

$\lambda(z;\varphi,p_x)$ having been defined in (2.14). The $\psi_s(z,\xi;\varphi,p_x)$ are simply the instants (previous to φ) at which a given trajectory crossed the plane $z=\xi$ of the metal plate before reaching the depth z at "time" φ, and they are shown explicitly in Fig. 3. The singularities in the integrand (2.22b) which occur whenever $v_z(\psi_s,p_x)=0$, i.e., whenever the effective region of a trajectory crosses the plane $z=\xi$, are eliminated by an integration by parts.

The surface impedance tensor $Z_{\alpha\beta}$ is defined by the following general expression[1]:

$$E_\alpha|_{z=0+}=(c/4\pi)Z_{\alpha\beta}(\mathbf{H}\times\mathbf{n})_\beta|_{z=0+}, \quad (2.24)$$

where $\mathbf{n}$ is the unit vector along the normal to the surface and $\mathbf{H}$ is the rf magnetic field near the surface. For an electric field which is transversely polarized with respect to $\mathbf{H}=H\mathbf{x}$ (see Fig. 1) the integrodifferential equation (2.20) reduces to

$$\frac{\partial^2 E(z)}{\partial z^2}=-i\int_0^d d\xi\, K(z,\xi)E(\xi), \quad (2.25)$$

where the y subscripts have been dropped; and the surface impedance (2.24) reduces to a scalar

$$Z(H)=i\frac{4\pi\omega}{c^2}\frac{E(z)}{\partial E(z)/\partial z}\bigg|_{z=0+}\equiv\frac{4\pi\omega}{c^2}(R+iX), \quad (2.26)$$

using the second of the curl equations (2.5). The quantities R and X in (2.26) have the dimensions of length and will be called the resistive and reactive skin depths, respectively.[28] Either R or X or both will be of the same order as the penetration depth of the field into the metal.

III. NUMERICAL MODEL

In order to solve the integrodifferential equation (2.25) numerically, the electric field distribution inside the metal plate will be calculated approximately at a finite mesh of points z_i, $i=1,\ldots,\nu+1$ (see Fig. 3), where the plate has been divided into ν (ν is an even integer) unequal divisions such that $z_1=0$ and $z_{\nu+1}=d$.

The density of the mesh is high near the surfaces or in the regions where the spatial variation of the electric field is expected to be large. The mesh is taken to be symmetrical about $z=\frac{1}{2}d$ in order to exploit the symmetry of the kernel $K(z,\xi)$ which results from the central symmetry of the Fermi surface $\mathcal{E}(-\mathbf{p})=\mathcal{E}(\mathbf{p})$:

$$K(z,\xi)=K(d-z,d-\xi). \quad (3.1a)$$

In terms of the symmetrical mesh just defined, (3.1a) becomes

$$K_{i,j}=K_{\nu+1-i,\nu+1-j}. \quad (3.1b)$$

The second derivative at the left-hand side of (2.25) evaluated at a point z_i of the coordinate mesh defined above is approximated numerically by a linear combination of functional values $E_j\equiv E(z_j)$ through a q-point differentiation formula[29]

$$E_i''=\sum_j A_{ij}E_j, \quad (3.2)$$

where the differentiation coefficients A_{ij} depend only on the coordinate mesh, and a polynomial of degree $(q-1)$ passing through the q points immediately closest to $E(z_i)$ has been assumed to approximate the curve $E(z)$ in that neighborhood ($q=3$ in the present calculations).

The integral of (2.25) is approximated by the quadrature formula (generalized trapezoidal rule for unequal spacings[29])

$$\int_0^d d\xi\, K(z,\xi)E(\xi)=\sum_{j=1}^{\nu+1} Q_j K_{ij}E_j, \quad (3.3)$$

where the quadrature weights Q_j depend only on the coordinate mesh and where the elements K_{ij} of the kernel $K(z,\xi)$, which depend on the magnetic field and contain all the physics of the problem, are given by the integrals over the Fermi surface in Eq. (2.21a). These integrals are evaluated numerically. For the integration over p_x we sum over all the slices normal to p_x in which the Fermi surface has been divided in such a way that the connectivity of the orbits in the kth slice is different from that of the $(k+1)$th slice; for example, the orbits in the kth slice may be closed and circular while they may be open, or they may have various other topologies, in the $(k+1)$th slice. For the integration over φ we sum over all the possible types of orbits, labeled by l, that the electrons describe for a given p_x and different directions of their velocities. The integrations over p_x for the kth slice and over φ for the lth orbit are carried out by using convenient quadrature formulas (Simpson's rule, for example[29]). Explicit use of this indexing of the orbits in order to carry out the calculation of $K(z,\xi)$ is made in Sec. IV C (see Fig. 11).

Using the approximations of (3.2) and (3.3), we can reduce the integrodifferential equation (2.25) to the following set of $(\nu-1)$ linear, algebraic equations:

$$\sum_{j=1}^{\nu+1} R_{ij}E_j=0, \quad i=2,\ldots,\nu, \quad (3.4)$$

[28] A. B. Pippard, *Electronics and Electron Physics* (Academic Press Inc., New York 1954), Vol. VI, p. 1.

[29] F. P. Hildebrand, *Introduction to Numerical Analysis* (McGraw-Hill Book Co., New York, 1956).

which are to be solved (by Gaussian elimination[29]) for the $(\nu-1)$ unknown values of the electric field $E_i=E(z_i)$, $i=2,\ldots,\nu$. The values of the field at the two surfaces $E_1\equiv E(0)$ and $E_{\nu+1}\equiv E(d)$ are assumed to be known from the experimental boundary conditions and the continuity of the tangential components of the electric field at a surface. From (3.2) and (3.3) the complex coefficients R_{ij} of (3.4) are simply

$$R_{ij}=A_{ij}+Q_jK_{ij}. \tag{3.5}$$

As soon as $E(z)$ is calculated at the finite mesh of points z_i for a magnetic field value H_1, the first derivative $\partial E/\partial z$ at the $z=0$ surface is approximated by a linear combination of E_i near $E(0)$, and the surface impedance at H_1 is calculated using (2.26).

To ensure numerical convergence for the above scheme, the spatial distribution of the points in the coordinate mesh can be varied until further changes in the mesh produce variations in $E(z)$ which are smaller than a given small amount. In doubling the total number of divisions (from $\nu=26$ to $\nu=52$, for example) so as to increase the mesh density either near the surfaces or in the interior of the sample, the large structure in the surface impedance above the nonresonant background suffers variations with respect to shape, position, and strength which are only of the order of 1% or less.

IV. MODEL CALCULATIONS AND RESULTS

In this section the formalism of Secs. II and III is used to calculate the electric field distribution inside a metal plate, of thickness $d=1.56\times10^{-2}$ cm, which has been excited by an electromagnetic field of frequency $\omega/2\pi=1$ MHz. From the calculated electric field distribution for different external magnetic field values, the approximate surface impedance of the plate is obtained as a function of the external magnetic field. This is done for various model Fermi surfaces and for different modes of excitation of the plate by the rf field. The only phenomenological parameter introduced in the formalism is the mean free path l which we take to be equal to the thickness of the plate.

The electric field at the two surfaces (normalized to unity for simplicity) is assumed to be real. Explicitly, the boundary conditions for the different modes of excitation are taken to be

(a) Bilateral, antisymmetric excitation:

$$\begin{aligned} E(0)&=1,\\ E(d)&=-1, \end{aligned} \tag{4.1a}$$

(b) Bilateral, symmetric excitation:

$$\begin{aligned} E(0)&=1,\\ E(d)&=1, \end{aligned} \tag{4.1b}$$

and (c) Unilateral excitation:

$$\begin{aligned} E(0)&=1,\\ E(d)&=0. \end{aligned} \tag{4.1c}$$

The boundary condition (4.1c) is not a good physical approximation, for it does not take into account the anomalous penetration of the field into the metal and neglects radiation at the second surface. We consider it, however, because in view of the linearity of the boundary conditions (4.1), it is trivial to construct the solution corresponding to (4.1c) by simply taking the average of the other two solutions [those corresponding to (4.1a) and (4.1b)]. This average solution produces a smooth variation of the surface impedance as a function of magnetic field, in disagreement with experiment. By assuming that an outgoing plane wave emerges at the $z=d$ surface, however, the correct solution for the unilateral mode of excitation can be constructed from Maxwell's equations in the plate and the boundary condition $E'(d)=i(\omega/c)E(d)$, which results from the continuity of the tangential components of the electric and magnetic fields at the second surface. The line shapes observed by Koch and Wagner[15] (using the single-sided geometry) in the surface impedance of potassium together with the RFSE transmission line shapes will be investigated in a subsequent paper.

A. Cylindrical Fermi Surface; Closed, Circular Trajectories

In this case the velocity of *every* electron has no component along the magnetic field and it is given simply by

$$\mathbf{v}=v_F(\mathbf{y}\cos\varphi+\mathbf{z}\sin\varphi), \tag{4.2}$$

where v_F is the Fermi velocity, which in the actual calculations has been taken to be 0.864×10^8 cm/sec, the Fermi velocity of electrons in potassium. For a given value of magnetic field all electron trajectories have the same size. The height of the Fermi surface cylinder is adjusted so that it gives the correct number of electrons (those in potassium again).

Several electric field distributions in the sample for the antisymmetric and symmetric modes of excitation are shown in Figs. 4 and 5, respectively, for certain characteristic values of the external magnetic field.

The calculated surface resistance R and surface reactance X, as functions of external magnetic field, are shown in Fig. 6 together with the derivatives $\partial R/\partial H$ and $\partial X/\partial H$, which are the experimentally measured quantities. The magnetic fields in the abscissas are in units of H_0, where H_0 is the critical value of the magnetic field for which one trajectory diameter exactly matches the thickness of the plate [$H_0=2(c\hbar/e)(k_F/d)=628$ Oe for $k_F=0.746$ Å^{-1} corresponding to the Fermi wave vector of potassium].

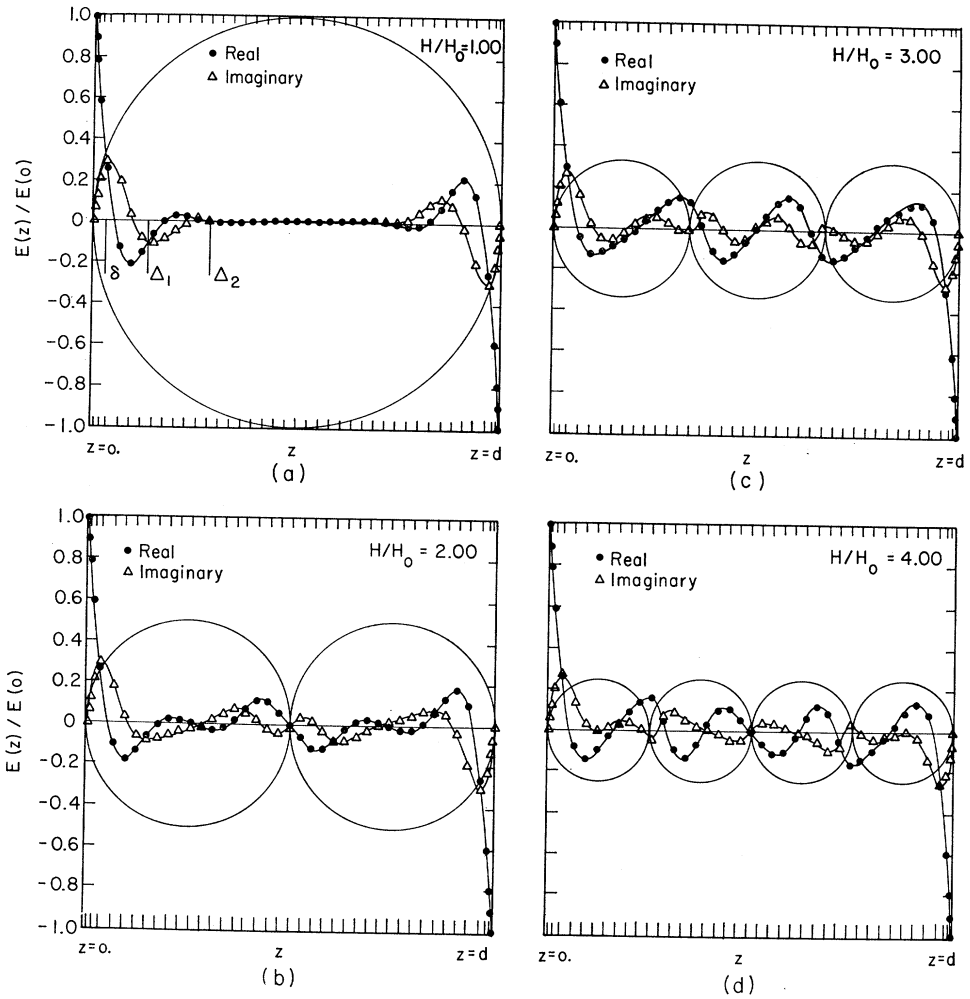

FIG. 4. Electric field distributions for various values of the external magnetic field; bilateral, antisymmetric excitation; cylindrical Fermi surface.

Certain characteristic features are to be noticed in the electric field curves of Figs. 4 and 5. The field near each surface damps rapidly into the sample with a penetration depth $\delta \approx 5.85 \times 10^{-4}$ cm, which is of the same order of magnitude as the average resistive or reactive depth of Fig. 6. In addition to this rapid (nearly exponential) decay within δ, the field has non-negligible structure for depths almost as large as ten times δ. As is discussed below, the two lengths $\Delta_1 \approx 4\delta$ and $\Delta_2 \approx 8\delta$, which are shown explicitly in Fig. 4(a), correspond to turning points in the sharp variation of the surface impedance with magnetic field. The general structure of the field near the surfaces is very much like the profile of the field in the anomalous skin-effect problem of a semi-infinite sample and in the absence of an external magnetic field.[30] This over-all surface structure of the electric field, because of the boundary conditions which fix $\mathbf{E}$ at $z=0$ and $z=d$, does not change significantly with H; however, the changes in the slope $\partial E/\partial Z$ at the surfaces, i.e., the rf magnetic field distribution near the boundaries, are very large, as demonstrated in Fig. 6 [see (2.26)].

The field distribution exhibits splashes, i.e., regions of nonzero amplitude, deep in the interior of the metal for $H/H_0 > 1$. The location of these splashes is roughly determined by the size of the effective electron trajectories. For $H/H_0 = 2$ for example, i.e., when two trajectory diameters completely fill the sample, the field splash is centered (antisymmetrically or symmetrically) around the middle of the plate. For this value of the magnetic field the size of the trajectories is such that an electron which couples effectively with the large amplitude field in either of the two skin layers has its other effective region (corresponding to $v_z = 0$) near the middle of the sample. The peak amplitude of the real part of this splash is about 0.1–0.15 of the amplitude at the surface, and the splash width is of the order of a few penetration depths. For higher values of magnetic

[30] T. W. Nee, J. F. Koch, and R. E. Prange, Phys. Rev. **174**, 758 (1968).

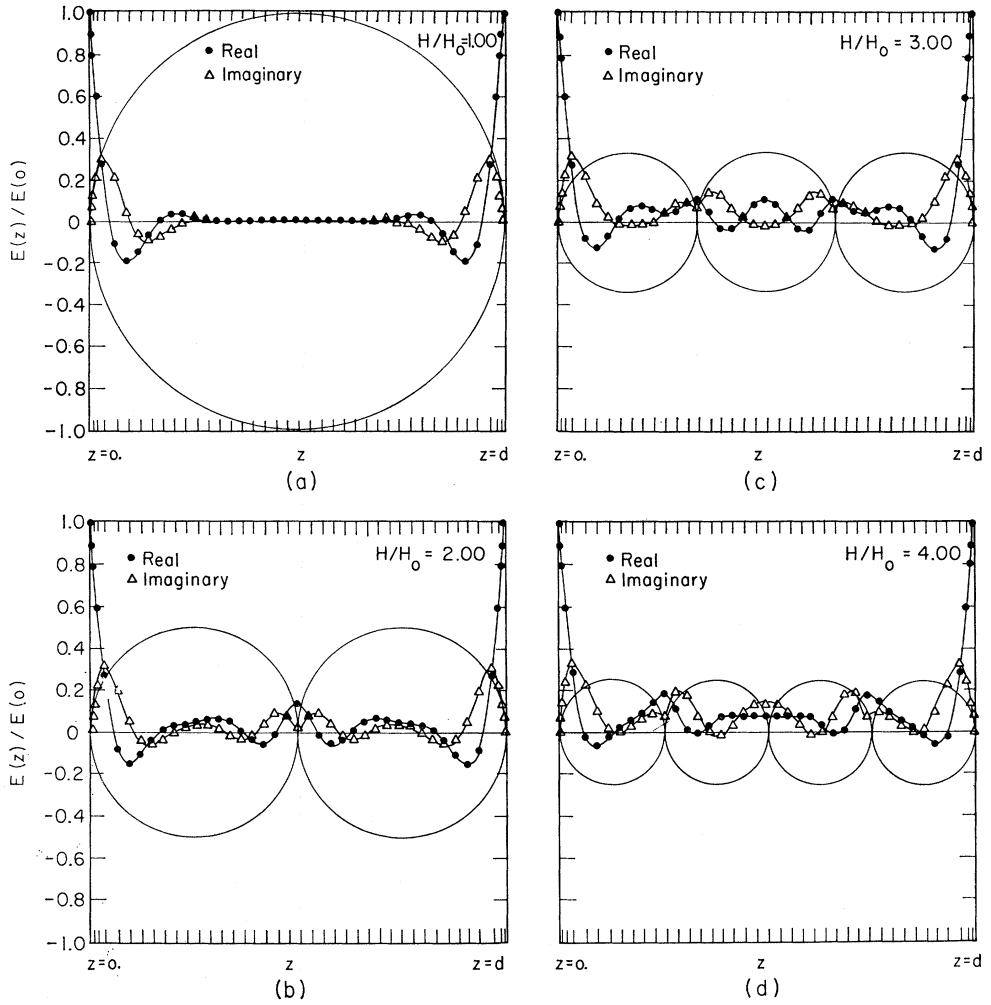

FIG. 5. Electric field distributions for various values of the external magnetic field; bilateral, symmetric excitation; cylindrical Fermi surface.

field, i.e., smaller size trajectories, the structure of the field in the bulk of the sample becomes even more complicated; the "trajectory chains" mentioned in the Introduction make new field and current splashes appear in different regions of the plate. Interference effects due to driving currents at both surfaces of the plate are, of course, always present.

The line shapes of Fig. 6 are reflections of the distribution of the electric field not only in the skin layers but in the interior of the sample as well; this is evidenced by the fact that singularities appear not only at $H/H_0=1$ but at higher values of external magnetic field as well. The resonances at higher fields appear approximately at $H/H_0=n$, where $n=2, 3\cdots$. The amplitude of these singularities decreases with their order n while their width increases, in accord with experiment.[8,31] In addition, the regions of sharp variation of the R curves seem to coincide with the extrema of the X curves, also in accord with experiment.[31,32]

The symmetry of the driving fields affects the singularities in a very obvious way. The surface impedance lines corresponding to the symmetric mode of excitation are reversed with respect to the lines of the usual antisymmetric mode of excitation. Such signal reversal was reported by Walsh.[20] This signal reversal is due to the fact that for a given magnetic field, say $H/H_0\geq 1$, the currents carried by the effective electrons from the one skin layer to the other add (subtract) to the driving currents of the second side for the antisymmetric (symmetric) mode of excitation. The constructive (descructive) interference between the transmitted and driving currents causes the initial decrease (increase)

[31] J. F. Koch and T. K. Wagner, Phys. Rev. **151**, 467 (1966).

[32] I. P. Krylov, Zh. Eksperim. i Teor. Fiz. Pis'ma v Redaktsiyu **1**, 24 (1965) [English transl.: Soviet Phys.—JETP Letters **1**, 116 (1965)].

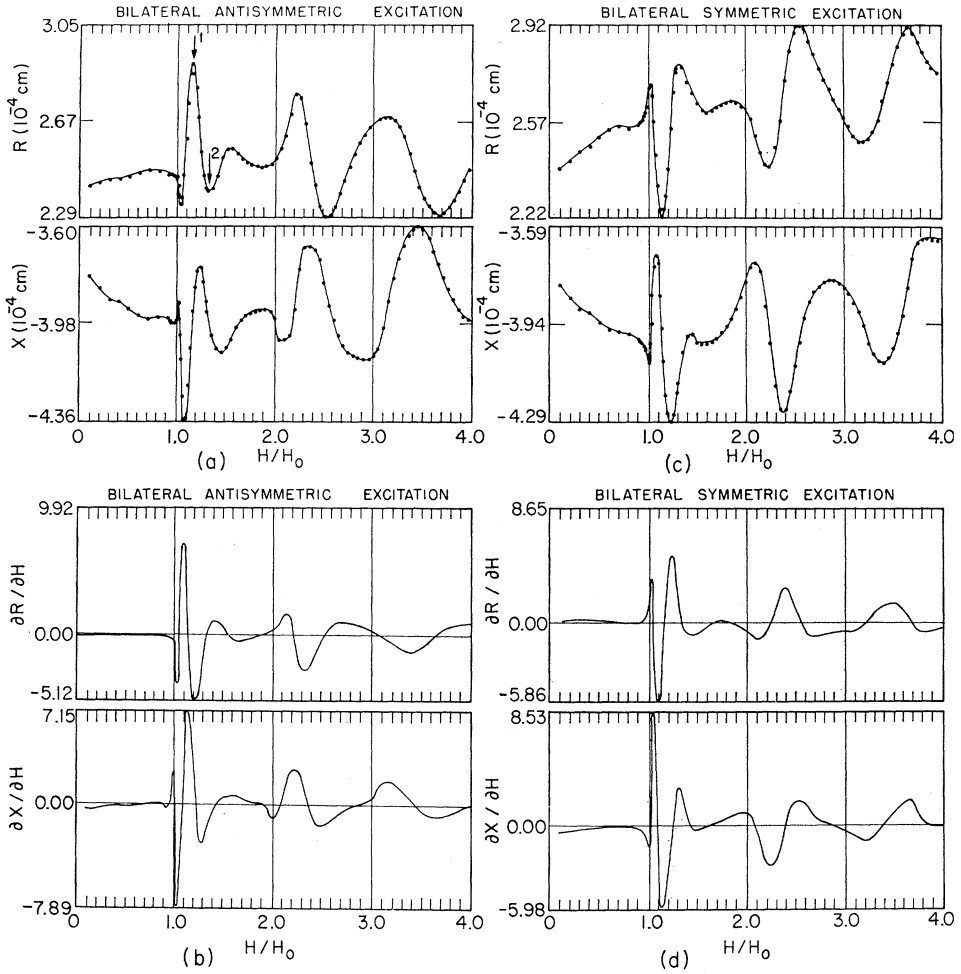

FIG. 6. Surface resistance R, surface reactance X, and their derivatives $\partial R/\partial H$ and $\partial X/\partial H$ as functions of external magnetic field for both bilateral, antisymmetric and bilateral, symmetric excitations. Cylindrical Fermi surface.

in the surface resistance R as a consequence of the increased (decreased) conductivity.

It should be mentioned here that, as a result of the opposing tendencies in the variation of surface impedance with magnetic field for the antisymmetric and symmetric modes of excitation, the magnetic field dependence of the impedance is much smoother in the mode of unilateral excitation, which we calculate as an average of the other two modes [see (4.1)]. As a consequence, this calculation does not give the correct line shape for the unilateral mode of excitation. By constraining the electric field to be zero at the $z=d$ surface, the very important influence of the transmitted currents upon the nature of the line shape is neglected, and the resonance near $H/H_0=1$ cannot reflect the emergence of the first field splash at the second surface.

For the bilateral, antisymmetric excitation the behavior of R, as shown in Fig. 6(a), can be discussed qualitatively in the following way. For $H/H_0<1$ the transport properties of the plate are dominated by orbits of the type shown in Figs. 2(b) and 2(c); this gives rise to a resistance that varies only very smoothly with H. The sharp decrease and subsequent increase in R between $H/H_0=1$ and $H/H_0=1.08$ is to be attributed to the relatively large number of effective trajectories of the type shown in Fig. 2(a). These trajectories, which interact effectively with the fields within both skin depths (as defined by $z=\delta$ and $z=d-\delta$), exist only in this range of magnetic fields. The diameter of the largest effective trajectory contributing to the initial dip is equal to d, while the diameter of the smallest contributing trajectory is equal to $d-2\delta$, approximately. This spread in effective trajectory diameters makes the linewidth of the dip mentioned above, $\Delta H/H_0\approx 0.08$, be approximately equal to $2\times\delta/d$. Thus, from the width of this resonance near $H/H_0=1$, a good estimate can be made for the skin depth.

The large peak in the surface resistance (bilateral, antisymmetric excitation) with a maximum at $H/H_0\approx 1.15$ appears in that range of magnetic field values for which the trajectories that interact effectively on the one skin layer (defined by $z=\delta$) do not pass through

the skin layer (defined by $z=d-\delta$) at the opposite surface; however, these trajectories do sample the field distribution near the second surface in regions of non-negligible structure [see Fig. 4(a)]. The diameter of the trajectories corresponding to the magnetic field value $H_1\approx 1.15H_0$ [at the peak maximum labeled by the first arrow in Fig. 6(a)] is equal to $d-\Delta_1$, while the diameter corresponding to $H_2\approx 1.30H_0$ [at the second minimum of R labeled by the second arrow in Fig. 6(a)] is equal to $d-\Delta_2$; Δ_1 and Δ_2 are defined in Fig. 4(a). The first peak in the surface resistance, then, reflects the distribution of the electric field between $z\approx\delta$ and $z\approx\Delta_2$. As is discussed below (Sec. IV B), it is the derivative of this peak that Koch and Wagner[31] measured in their experiment on potassium. For an electron starting within the depth $z=\delta$, where the real part of the electric field is large and positive and the imaginary part is almost zero, the real part of the product $\mathbf{v}\cdot\mathbf{E}$ which couples the electronic motion with the electric field [see Eq. (2.16a)], is large and positive. For magnetic fields in this range, this electron will interact with the field near the second surface in the region between $z=d-\delta$ and $z=d-\Delta_2$, where the coupling product is now negative and the imaginary part of the field takes its largest values. This interference between the transmitted currents from the one surface and the driving currents at the second surface (for depths larger than δ) is destructive for magnetic field values in this range and it causes the peak in R, while the constructive interference between the transmitted and driving currents (for depths less than δ) is the primary cause for the initial dip in R.

For the peaks in R (bilateral, antisymmetric excitation) with maxima at $H/H_0\approx 2.22$ and $H/H_0\approx 3.10$, similar geometric arguments could be advanced if one took into account the electric field splashes inside the sample in addition to the skin layers. However, these arguments are not easy to make quantitatively; the secondary "skin depths" in the bulk of the sample cannot be precisely defined since they "move" self-consistently with the field (see Fig. 4).

Of course, such simplified arguments in terms of the coupling product $\mathbf{v}\cdot\mathbf{E}$ for an effective electron are already included in the general expressions of Sec. II, where the contributions from *all* the effective electrons as well as *all* the ineffective ones are properly integrated over [see Eq. (2.17)]. In this connection, we note that the surface impedance is an integral property of the total electron distribution; the resonant electrons only perturb the over-all conductivity of the plate.[33]

The diffuse scattering at the surfaces determines mostly the position of the first sharp variation at $H/H_0=1$. The effect of surface scattering on the relative population of effective-versus-ineffective electrons is maximum for magnetic field values immediately after $H/H_0=1$; then, the trajectories of the type shown in Fig. 2(c) cease to exist and the trajectories of the type shown in Fig. 2(a) appear for the first time.

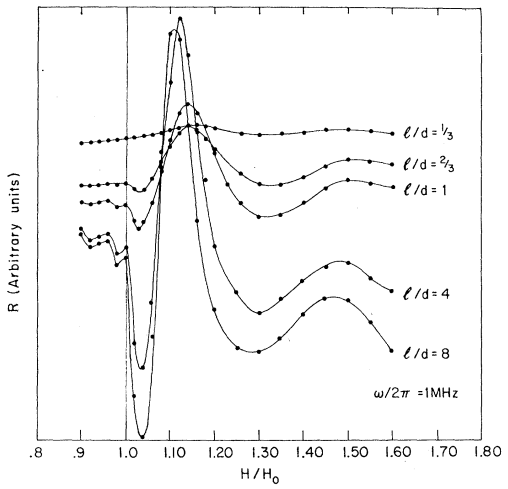

FIG. 7. Mean-free-path dependence of the surface resistance. Bilateral, antisymmetric excitation; cylindrical Fermi surface.

The effect of specular scattering on the line shapes will be examined in a subsequent investigation. For different magnetic field values and different frequency ranges one may have to use a combination of the two scattering mechanisms in order to make explicit comparison with experiment.

The collisions in the bulk, described by the mean free path l, affect not only the intensity of the lines but their shape as well. This is seen in Fig. 7, where the surface resistance for the bilateral antisymmetric excitation has been plotted as a function of magnetic field (near $H/H_0=1$) for different ratios of l/d, ranging from $l/d=\frac{1}{3}$ to $l/d=8$. As the l/d ratio decreases from $l/d=1$ to $l/d=\frac{1}{3}$, the initial dip in the surface resistance (between $H/H_0=1$ and $H/H_0=1.08$) gradually disappears while the subsequent peak still persists, although damped considerably. This demonstrates that the important influence of the mean free path is that it affects the effectiveness of the electrons in bringing currents from the one skin layer to the second. The part of the line (initial dip) which reflects the constructive interference between the driving currents (in the region within δ of the first surface) and the transmitted currents from the corresponding skin layer at the second surface is washed out faster than the parts of the line (first peak) which are mediated by smaller-size trajectories. As the ratio l/d increases from $l/d=1$ to $l/d=8$, the initial dip in R increases considerably in amplitude (almost by a factor of 10), while the subsequent peak increases at a smaller rate. In addition to the large variation in amplitude, there is a shift in the position of the first maximum towards smaller magnetic field values as l/d increases. The shift in the position of the first minimum is almost negligible. As the ratio l/d decreases, the line shows a general broadening

[33] R. G. Chambers, Proc. Phys. Soc. (London) **86**, 305 (1965).

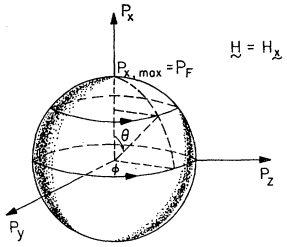

FIG. 8. Spherical Fermi surface. The real-space trajectories for a given p_x, other than $p_x=0$, are helical in nature; their projections on planes normal to **H** span the sample as shown in Figs. 2(a)–2(c).

which is larger in the resistance peak than it is in the preceding resistance dip. These observations regarding the mean-free-path dependence of the line shape will be useful in the qualitative understanding of the observed line shapes in potassium (see the discussion in Sec. IV B).

The background surface resistance and surface reactance are related by the well-known relation

$$X \approx -\sqrt{3}R,$$

which has been derived for the anomalous skin-effect problem in the semi-infinite metal and in the absence of external magnetic fields.[6]

The critical value of the magnetic field H_0 corresponds to the first (i.e., leftmost) sharp variation of the line, as has been correctly assumed to be the case in the experimental works that measured calipers of Fermi surfaces using the RFSE as a spectroscopic tool (see Ref. 9, for example).

B. Spherical Fermi Surface

For a spherical Fermi surface the velocity of the electrons is given by (see Fig. 8)

$$\mathbf{v} = v_F(\mathbf{x}\cos\theta + \mathbf{y}\sin\theta\cos\varphi + \mathbf{z}\sin\theta\sin\varphi). \quad (4.3)$$

For a given p_x, i.e., θ, the real-space trajectories are, in general, helices. The velocity (4.3) has a component along the magnetic field for all values of p_x, except $p_x=0$, which corresponds to the stationary "belly"

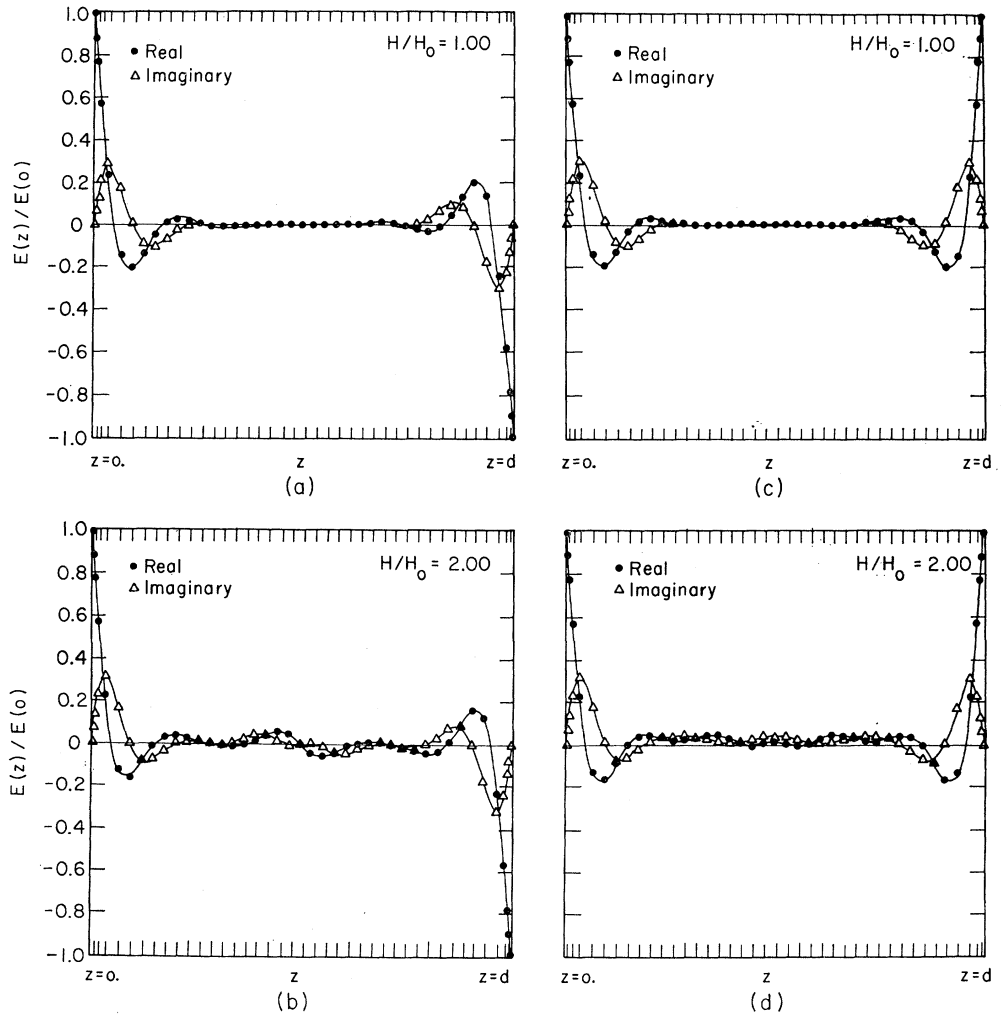

FIG. 9. Electric field distributions for various values of the external magnetic field and both modes of excitation (bilateral, antisymmetric and bilateral, symmetric) by the rf field. Spherical Fermi surface.

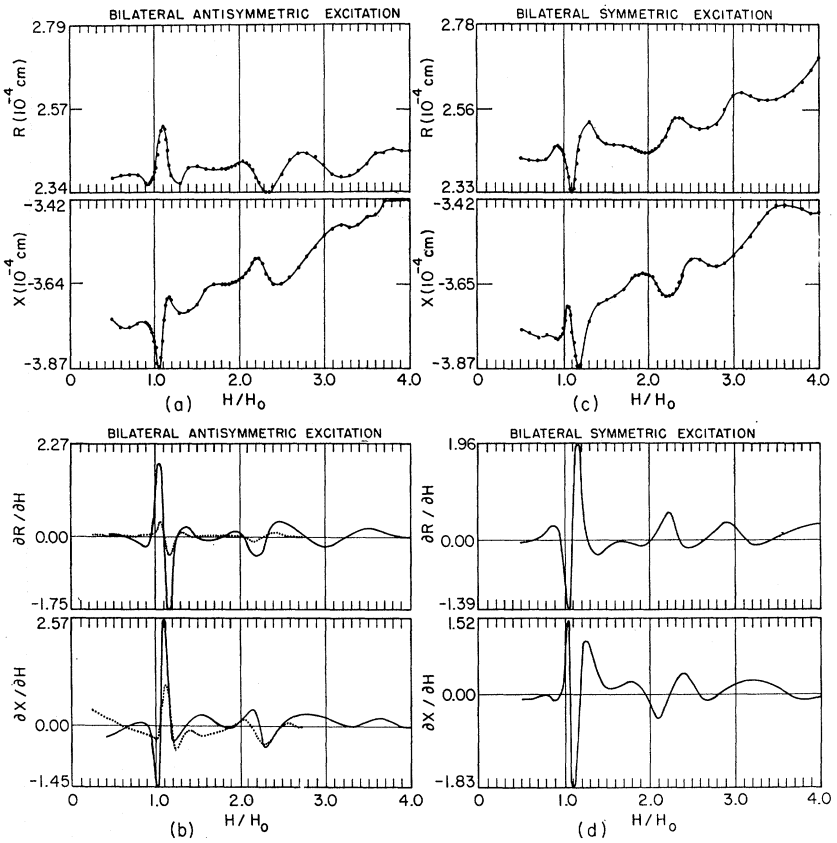

FIG. 10. The surface resistance R, surface reactance X, and their derivatives $\partial R/\partial H$ and $\partial X/\partial H$ as functions of external magnetic field for both bilateral, antisymmetric and bilateral, symmetric excitations. Spherical Fermi surface. The dotted curves in (b) are experimental (see Ref. 15).

orbit at the equator of the Fermi sphere. Since the magnetic field has been chosen to be parallel to the surface of the sample, the electron trajectories return to the same depths for a given value of the external magnetic field, and, even though they are helical in nature, it is convenient to visualize them as spanning the plate in the way depicted in Fig. 3.

The electric field distributions and the surface impedance curves are shown in Figs. 9 and 10. The normalization field H_0 is defined by the diameter of that "belly" trajectory which spans the plate exactly once. Because there is a large dispersion in the sizes of possible trajectories [ranging in diameter from zero at the limiting points of the Fermi distribution to $2(c\hbar/e)k_F/H$ at the "belly" orbit], the amplitudes of the field splashes are small and their widths large. The over-all intensity of the lines of the surface impedance is decreased considerably in this case as compared with the intensity of the lines in the cylindrical Fermi-surface case, as expected. The lines are also shifted slightly to the left, as compared with the corresponding cylindrical Fermi-surface lines, owing to the fact that for magnetic field values smaller than a given critical value, say $H/H_0=1$, there exist smaller trajectories in the neighborhood of the extremal trajectory which interact effectively with both skin layers.

The field derivatives of the surface impedance (bilateral, antisymmetric excitation) are shown in Fig. 10(b) together with the lines experimentally observed in potassium by Koch and Wagner.[31] Any comparison between the theoretical and experimental curves is meant to be only qualitative, for the following reasons. The experimental mean free path is given in Ref. 15 as $l\approx 6\times 10^{-3}$ cm with $l/d\approx\frac{1}{3}$. The mean free path used in this calculation was equal to the thickness of the plate, i.e., $l/d=1$. The small experimental l/d ratio has the following unfortunate consequence. Even in the cylindrical Fermi-surface case, as was discussed in Sec. IV A and shown in Fig. 7, the amplitudes of the surface impedance lines reduce by a large factor as the l/d ratio decreases from $l/d=1$ to $l/d=\frac{1}{3}$. Such a decrease in line amplitude is considerably more pronounced in the case of the spherical Fermi surface, where the signal is so reduced that the calculated variations of the surface impedance are buried in the numerical noise of the present calculation. Thus, an explicit calculation using Koch and Wagner's experimental parameters was regrettably inaccurate. In addition, the experimental curves in Fig. 10(b) were taken at $\omega/2\pi=1.5$ MHz, while the calculations were carried out at $\omega/2\pi=1.0$ MHz; such a difference in frequency, however, would only slightly affect the widths of the lines, leaving their shapes essentially unaltered for qualitative purposes. In view of these

differences between the experimental and calculational parameters, the vertical scale for the calculated curves has not been adjusted so as to bring them in closer correspondence with the experimental ones.

The qualitative similarity between the theoretical and experimental line shapes is rather good not only for the first large singularity at $H/H_0\approx 1$ but for the second harmonic as well. From the study made in Sec. IV A on the l/d dependence of the surface resistance line at $H/H_0\approx 1$, the first dip in the surface resistance of Fig. 10(a) would tend to disappear as l/d reduces from $l/d=1$ to $l/d=\frac{1}{3}$; only the subsequent peak in the surface resistance would remain, thus yielding a derivative that would agree even more closely with experiment. Similar qualitative arguments could be advanced about the agreement of the $\partial X/\partial H$ curve with experiment.

In terms of these qualitative arguments one might discuss by extrapolation the disturbing difference which exists between the $\partial R/\partial H$ curve which was measured by Koch and Wagner[31] in potassium and that which was measured by Peercy *et al.*,[34] also in potassium. The explanation for the difference between the two line shapes might lie in the rather strong mean-free-path dependence of the line shape and very likely on the nature of surface scattering for large mean free paths.

In the first experiment[31] the relevant parameters were $l/d\approx\frac{1}{3}$, $\omega/2\pi=1.5$ MHz, and $\omega\tau\approx 0.0006$. From the l/d dependence of the line shape shown in Fig. 7, it is fair to say that this experiment measured the derivative of the first peak in the surface resistance, since the initial dip might be suppressed because of the small mean free path. In terms of the arguments put forth in Sec. IV A, which attribute this peak to the coupling of effective electrons with the part of the electric field distribution extending beyond δ, i.e., beyond the first exponential decay of the field, one can understand the large width (a few times δ) of the observed lines.

In the second experiment[34] the relevant parameters were $l/d\approx 4$, $\omega/2\pi=32.694$ MHz, and $\omega\tau\approx 0.1$. In this case, the observed $\partial R/\partial H$ line exhibits a very large dip immediately after $H/H_0=1$ which would result from a (negative) steplike discontinuity at $H/H_0=1$ in the surface resistance, without the subsequent large structure which is so predominant in our calculations. It might be, however, that the assumption (2.11c), which we have made in our calculations, is no longer valid for $\omega\tau\approx 0.1$. This large $\omega\tau$ (more than two orders of magnitude larger than the $\omega\tau$ of the first experiment and of our calculations) might affect the phase of the electric field, in the regions beyond δ and for time intervals comparable to the relaxation time, so as to change the character of the interference between the driving and transmitted currents and thus to wash out some of the large peak in R. In addition, because of the large mean free path of this experiment it might make a difference whether the scattering at the surface is diffuse, as we have assumed in our calculations, or specular—at least for those trajectories which scatter at the surfaces with small angles of incidence. In this connection, we mention the importance of the specularly reflected "skipping" trajectories in the microwave surface impedance at low magnetic fields.[25] So, in order to explain the line shapes observed in the second experiment, an explicit calculation is needed that would include possible finite $\omega\tau$ effects and, perhaps more importantly, different assumptions about the nature of surface scattering. In such a calculation the line shapes observed in the tilted field geometry will be investigated as well.

C. Undulating Cylinder Fermi Surface

The undulating cylinder Fermi surface which includes the deformation of the free-electron sphere near the Brillouin-zone boundaries is shown in Fig. 11. The types of trajectories that the electrons describe in the sample for a particular orientation of **H** with respect to the symmetry axes of the crystal are also shown in Fig. 11. The Fermi surface has been divided into two p_x slices, labeled by the index k. In the first slice ($k=1$), where $p_{x,c}<|p_x|\leq p_F$, the trajectories are closed and circular for all directions of their velocity, i.e., for $0\leq\varphi<2\pi$. In the second slice ($k=2$), where $0\leq|p_x|<p_{x,c}$, three types of trajectories, labeled by the index l, are possible for different ranges of φ, i.e., for different velocity directions, (i) open, for $2\pi-\varphi_c\leq\varphi\leq\varphi_c$, $v_y(\varphi)>0$ ($l=1$); (ii) closed, lenslike, for

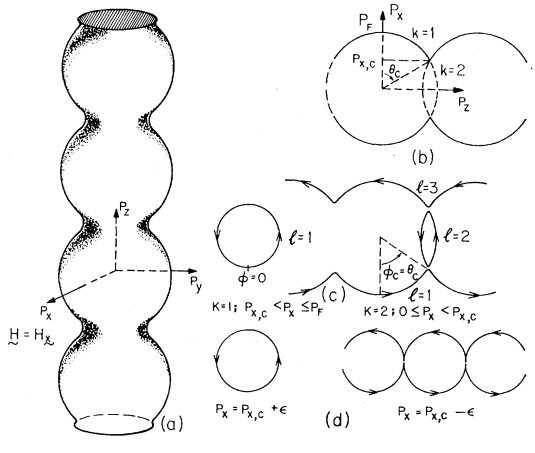

FIG. 11. (a) Undulating cylindrical Fermi surface which includes the deformation of the free-electron sphere near a Brillouin-zone boundary. (b) Definition of $p_{x,c}$, θ_c, and the two p_x slices labeled by k. (c) Classification of the orbits in a magnetic field. In $k=1$ ($p_{x,c}<|p_x|\leq p_F$), the orbits are all of one type; closed and circular. In slice $k=2$ ($0\leq|p_x|<p_{x,c}$), there are three types of orbits, labeled by l, for different directions of the electron velocity: open orbits ($l=1, 3$) and lenslike ($l=2$). (d) The nature of the orbits near the transition section $p_x=p_{x,c}$.

[34] P. S. Peercy, W. M. Walsh, Jr., L. W. Rupp, Jr., and P. H. Schmidt, Phys. Rev. **171**, 713 (1968).

$\varphi_c \leq \varphi \leq \pi - \varphi_c$ and $\pi + \varphi_c \leq \varphi_c \leq 2\pi - \varphi_c$ $(l=2)$; (iii) open, for $\pi - \varphi_c \leq \varphi \leq \pi + \varphi_c$, $v_y(\varphi) < 0$ $(l=3)$. The velocities of the electrons in each piece of their trajectory are given by (4.3). At the zone boundaries we take

$$v_y(\varphi_c,\theta) = -v_y(\pi - \varphi_c, \theta) = v_F \sin\theta,$$
$$v_z(\varphi_c,\theta) = v_z(\pi - \varphi_c, \theta) = 0. \tag{4.4}$$

The electric field distributions inside the plate and the surface impedance as a function of magnetic field, for this Fermi surface are shown in Figs. 12 and 13, respectively. At the value H_0 of the external magnetic field the circular orbit corresponding to the transition section of the Fermi surface, defined in Fig. 11(d), matches the thickness of the sample, i.e.,

$$H_0 = 2(c/e)p_{z,c}/d. \tag{4.5}$$

This choice was made in order to emphasize the large variation of the impedance curves observed in cadmium, whose Fermi surface this undulating cylinder model is supposed to approximate, near this value of the field.[9]

The variety of possible trajectories for different directions of the electronic velocity and the different ways in which the various trajectories span the sample contribute to the increased complexity of all curves. Owing to their different topologies, different trajectories contribute to the conductivity in different ways. Because of their shape and the way in which they are located with respect to the sample, the various trajectories have different degrees of efficiency in bringing currents from one surface layer to the other and also in affecting the relative populations of effective and ineffective electrons. The observed peaks in the surface resistance and reactance correspond roughly to the geometric matching of the important trajectories with the thickness of the sample. The high magnetic field peaks are due to the anomalous penetration of the field in the sample brought about by multiple trajectory

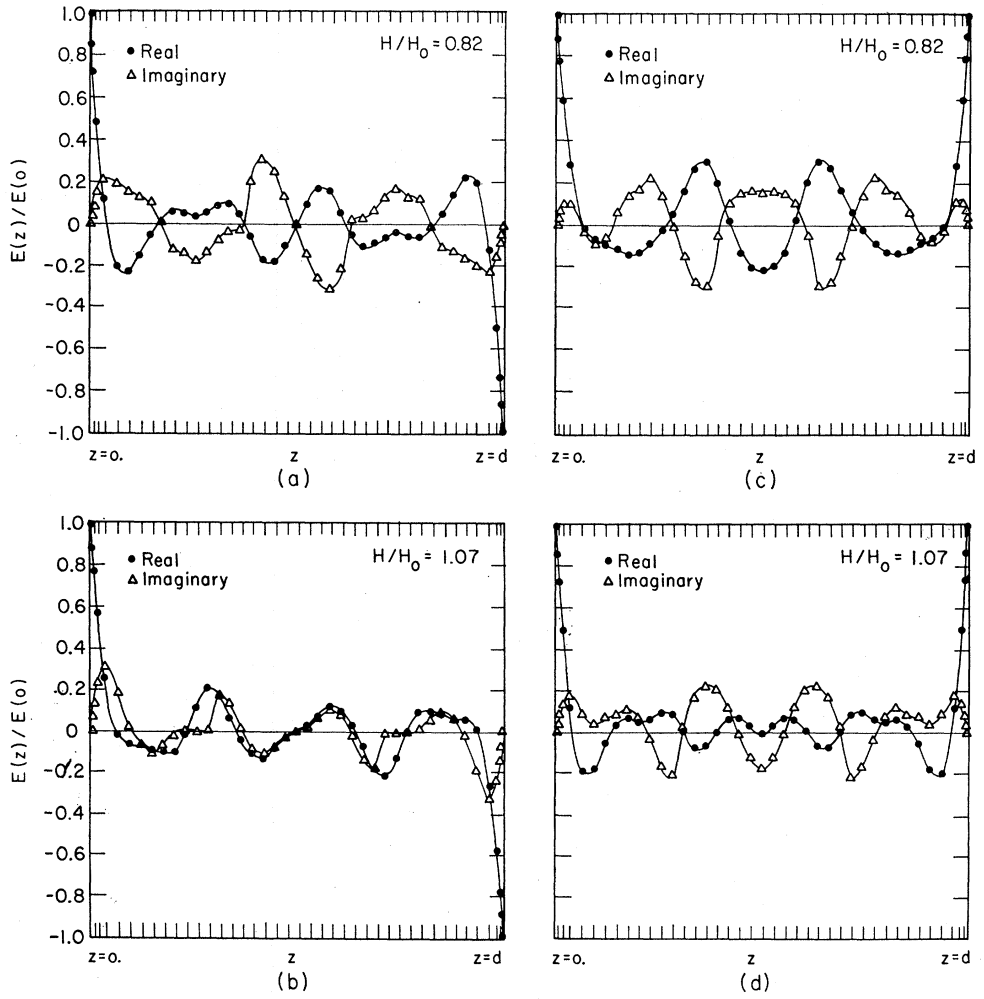

FIG. 12. Electric field distributions for various values of the external magnetic field and both modes of excitation (bilateral, antisymmetric and bilateral, symmetric) by the rf field. Undulating cylinder Fermi surface.

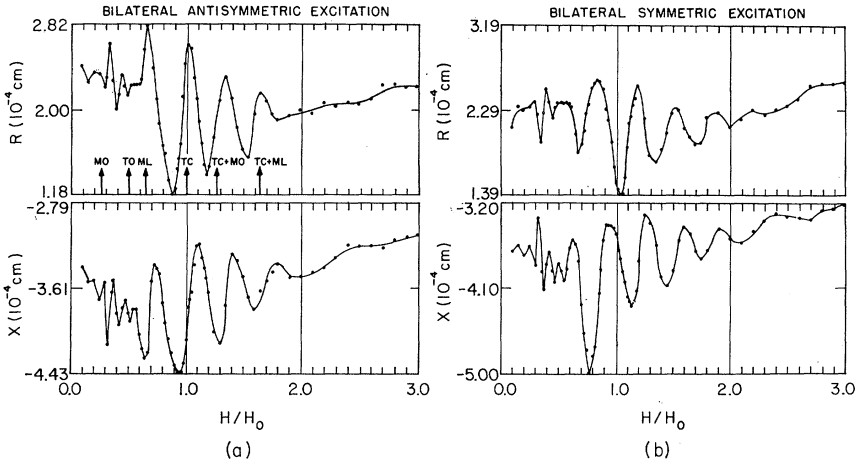

FIG. 13. The surface resistance R and the surface reactance X as functions of external magnetic field for both bilateral, antisymmetric and bilateral, symmetric excitations. Undulating cylinder Fermi surface.

chains. The critical fields at which certain characteristic trajectories (or chains of trajectories) completely fit the sample are shown explicitly in Fig. 13(a) by means of arrows. A classification of these characteristic trajectories follows: (i) MO is the open trajectory [of the type $k=2$, $l=1$ or 3 in Fig. 11(c)] at the maximum section of the Fermi surface $p_x=0$; $H_{\mathrm{MO}}=0.27H_0$. (ii) TO is the open trajectory [shown in Fig. 11(d)] at the transition section $p_x=p_{x,c}$; $H_{\mathrm{TO}}=0.5H_0$. (iii) ML is the lens trajectory [labeled by $k=2$, $l=2$ in Fig. 11(c)] at the maximum section; $H_{\mathrm{ML}}=0.64H_0$. (iv) TC is the closed, circular trajectory [shown in Fig. 11(d)] at the transition section; $H_{\mathrm{TC}}=H_0=528$ Oe for $\varphi_c=\theta_c=1$ rad [see Fig. 11(c)]. (v) TC+MO and TC+ML are trajectory chains made up of the closed, circular orbit at the transition section and the open or lens orbit, respectively, at the maximum section of the Fermi surface.

We may assume that the structure in the $Z(H)$ curves between H_{MO} and H_{TO} in Fig. 13 is primarily due to the open orbits since they are the only trajectories in this range of magnetic fields that interact effectively with both skin layers. The structure beginning at H_{ML} might be attributed to the lens orbits, and similar assignments can be made for the other peaks; however, this kind of assignment cannot be made rigorously in view of the considerable complexity of the field distribution deep inside the sample (see Fig. 12).

V. CONCLUSION

Although the numerical procedure of Sec. III is only approximate, it does provide a straightforward, but nevertheless self-consistent, approach to the rather formidable boundary-value problem of the anomalous skin effect in thin metallic samples with external magnetic fields present. From the preliminary model calculations of Sec. IV we obtain a satisfactory interpretation of the calculated (and in one instance of the experimental) line shapes of the RFSE in terms of the complete solution to the full boundary-value problem. By optimizing the numerical approximations of the model one could possibly carry out more accurate calculations with realistic Fermi surfaces that would make more effective the use of the RFSE as a spectroscopic tool. Explicit comparison with experiment might also improve our understanding of the nature of electronic scattering at the surfaces. Calculation of the RFSE, using an extension of this model, for external magnetic fields tilted with respect to the surface of the plate might help elucidate the many singularities that appear in the surface impedance due to electrons drifting from the surfaces of the plate to the bulk. As a limiting case of such a calculation, the impedance oscillations observed for external magnetic fields normal to the surface of the plate could be investigated. The nonmonotonic (and not explained as yet) behavior of the surface impedance at low magnetic fields and radio frequencies[25] could also be examined by using a variation of this model and by properly introducing the effect of the skipping orbits, if any.

ACKNOWLEDGMENTS

I want to express my deep gratitude to Professor L. M. Falicov for suggesting this problem and for his patient guidance and encouragement during the execution of this research. In addition, I want to acknowledge discussions with my colleagues at the James Franck Institute. In addition to the direct financial support by the U. S. Office of Naval Research and the National Aeronautics and Space Administration, this work benefited from general support to the Materials Sciences at the University of Chicago by the Advanced Research Projects Agency.